Journal of the Brazilian Society of Mechanical Sciences and Engineering (2023) 45:538
https://doi.org/10.1007/s40430-023-04452-y

TECHNICAL PAPER

Experimental analysis and numerical simulation of the behavior of smart sandwich beams in magnetorheological elastomer–honeycomb

L. Guenfoud[1] · N. Chikh[1] · S. Aguib[1] · T. Djedid[1] · L. Kobzili[1] · A. Nour[1] · M. Meloussi[1]

Received: 1 May 2023 / Accepted: 28 August 2023 / Published online: 24 September 2023

Abstract
Composite structures based on magnetorheological elastomers are widely used in many industrial sectors, such as the automotive, naval, railway, aeronautical, aerospace, and building industries because of their adjustable mechanical properties by an external stimulus. In this work, the experimental tests and the numerical simulation carried out have shown that the use of these new structures, developed from a honeycomb core and a MRE core with aluminum skins, makes it possible to improve in a particular way the overall rigidity and to reduce the vibration amplitudes. The results showed that these new hybrid structures have a very good mechanical resistance due mainly to the honeycomb core and a very good shock absorber due mainly to the core of the magnetorheological elastomer. The elaborated composite structure is intended to be used in industrial sectors subject to great efforts and a high amplitude of vibration such as helicopter wings and air turbines.

Keywords Hybrid sandwich structures · Magnetorheological elastomer · Honeycomb · 3-point bending · Mechanical strength · Damping

List of symbols

MRE	Magnetorheological Elastomer
ERV	Representative Elementary Volume
CIP	Carbonyl Iron Powdered
FNN	Feedforward Neural Network
MAE	Magneto-Active Elastomers
FRP	Fiber-Reinforced Polymer
CNT	Carbon NanoTubes
MWCNT	Multi-Walled Carbon NanoTubes
FMH	Fiber-Metal Hybrid
FGPE - MRE	Functionally Graded Piezoelectric layers-Magneto-Rheological Elastomer
θ	Cell angle
ϕ	Cell diameter
h	Wall thickness
$t, t^{/}$	Vertical and inclined wall thickness
a, b	Length and width of honeycomb
E_h	Young's modulus of honeycomb
E_s	Young's modulus of skin
E_{MRE}	Young's modulus of magnetorheological elastomer
ρ_h	Honeycomb density
ρ_s	Skin density
ρ_{MRE}	Magnetorheological elastomer density
ν_h	Poisson's ratio of honeycomb
ν_s	Poisson's ratio of skin
ν_{MRE}	Poisson's ratio of magnetorheological elastomer
U_{int}	Internal strain energy
u_h	Displacement along the x-axis of a vertical wall
v_h	Displacement along the y-axis of a vertical wall
u_h	Displacement along the x-axis of an inclined wall
v_l	Displacement along the y-axis of an inclined wall
ε_{xh}	Deformation along the x-axis of a vertical wall
ε_{yh}	Deformation along the y-axis of a vertical wall
ε_{xl}	Deformation along the y-axis of an inclined wall

Technical Editor Samikkannu Raja.

✉ S. Aguib
s.aguib@univ-boumerdes.dz

[1] Motor Dynamics and Vibroacoustics Laboratory, M'Hamed Bougara Boumerdes University, Boumerdes, Algeria

ε_{yl}	Deformation along the x-axis of an inclined wall
γ_{xyh}	Angular deformation of an inclined wall
γ_{xyl}	Angular deformation of an inclined wall

1 Introduction

To improve the performance of the mechanical behavior of structures, engineers make several efforts to design structures with good rigidity, high mechanical strength, high damping and great lightness. Sandwich structures made of composite materials respond well to certain requirements but still remain insufficient. Today, there is a class of so-called smart magnetorheological elastomer (MRE) composite materials that perfectly meet these requirements. Most of the existing works in this field are dedicated to the development and analysis of the mechanical behavior of the MRE, we cite among others the following works, Janbaz et al. [1]. In the latter, the authors have developed a mathematical model to determine the elastomer constants of a magneto-hyper-viscoelastic constitutive model, this model is based on uniaxial compression tests, and on impact resistance tests in the presence and in the absence of a magnetic field. The results showed that the constitutive properties of MRE strongly depend on the frequency, amplitude, duration of the applied stress and magnetic field. Dargahi et al. [2] were based on the study of the static and dynamic properties of magnetorheological elastomers as a function of the magnetic field density; the results revealed a 1672% increase in the storage modulus of the MRE when subjected to a magnetic field of 450 mT, which shows the potential of the new MRE to control vibrations and noises in various technical applications. Bernat et al. [3] discussed the current new trends of MRE applications in the field of advanced automation systems and robotic systems. The study done by Khairi et al. [4] examined the effect of silicone oil plasticizers on the magnetorheological materials properties. It showed that the incorporation of silicone oil reduces the rigidity and increases the response to magnetic field. Moreover, the study also showed that the introduction of CoFe2O4 improves magnetic properties, hardness and storage modulus. Bhaktha et al. [5] experimentally studied the viscoelastic properties of MRE in sandwich beam configuration using the ASTM E756-05 standard. Their studies depend on the percentage change in CIP and magnetic flux density. The obtained results show that the increase in the latter causes an increase in the shear modulus and the loss factor and that the magnetic attraction causes a phenomenon of static deflection, which leads to a decrease in the natural frequencies of the structure. Keshav et al. [6] focused their work on optimizing the geometry of the magnetic circuit by maximizing the magnetic flux density in the MRE region. To do this, a prediction neural network (FNN) was used to analyze the distribution of the magnetic field according to different geometric dimensions of the magnetic circuit, the results of the proposed model showed that the distribution of the magnetic field is predicted at about 30–50%, which is considered approximate for a real-time application. Moreno-Mateos et al. [7] have developed a new solution based on hybrid magnetorheological elastomers. They used a mixture of soft and hard magnetic particles to improve the performance of magnetorheological elastomers, which can be used to design flexible and versatile actuators. A simulation of bimorph beam shows how these hybrid MRE can improve mechanical flexibility and stiffness as a function of the magnetic field. Makarova et al. [8] investigated the possibility of creating an effective retinal fixative using magneto-active elastomers (MAE) and permanent magnet systems. The results of the study show that it is possible to use MAE as part of a magnetic fixator to treat complicated retinal detachments. Saxena et al. [9] in their work, they present a theory to model magneto-viscoelastic nonlinear deformations. The dissipation mechanisms have been taken into account by decomposing the strain gradient and the magnetic induction into elastic and viscous parts. In their work, Wang et al. [10] studied the mechanical properties of magnetorheological elastomers with an angle of inclination in compression mode, as well as the dynamic mechanical properties under different strain amplitudes and frequencies. The experimental results showed that the magnetically induced stress range decreases when the magnetic chain inclination angle increases, and the magnetically induced modulus decreases when the magnetic chain inclination angle is larger. Nedjar et al. [11] presented an experimental analysis of the magnetorheological behavior of elastomeric composites under dynamic loading. The elastomer is 40% infilled with ferromagnetic particles. The characterization of the rheological properties has been performed and the relationship between the ferromagnetic particles percentage weight and the applied magnetic field has been studied. The results found show that this composite has a high energy dissipation, further accentuated by the structure and the magnetic field. Some works have been done on MRE structures, and very little works are done on MRE-honeycomb structures, among these works are the following, Felipe de Souza Eloy et al. [12], in their work, they combined composite materials with an MRE core. They demonstrated that this combination of composite materials, honeycomb core and MRE is an excellent method to reduce vibrations, because it allows changing the modal parameters of the structure without affecting its mass. Wang et al. [13] evaluated the mechanical performance of MRE sandwich plates with four types of different panel materials, namely fiber-reinforced polymer (FRP), fiber-reinforced polymer with carbon nanotubes (CNT-FRP), metal and fiber-metal hybrid (FMH) panels. A theoretical model has been

proposed. This model will make it possible to determine the static rigidity, the dynamic rigidity, and the damping. The results found showed that the four types of structures possess excellent passive damping and stiffness properties, even without the application of an internal magnetic field. Selvaraj et al. [14] performed a dynamic analysis to evaluate the natural frequencies and damping ratios of laminated composite sandwich beams with a magnetorheological elastomer core reinforced with multi-walled carbon nanotubes (MWCNT-MRE) under different magnetic fields and boundary conditions. The experimental and numerical results show that the incorporation of CNT in the MRE gives high stiffness and also improves the damping characteristics of the structure. Liu et al. [15] propose a modeling method by the feedback control law. This modeling aims to show the compressibility and characterize the failure of the active–passive damping of the magnetorheological elastomer core of the piezoelectric sandwich plate (FGPE-MRE). Dai et al. [16] exploited the point interpolation method to evaluate the vibrations of a conical sandwich panel with a magnetorheological elastomer or electrorheological elastomer core and sheets made of composite materials. The results of their study showed that several factors such as the number of surface layers, the thickness, the pattern of the composite layers, the weight fraction and the electric/magnetic field, as well as the geometry of the conical panel, have a significant impact on the natural frequency of the system as well as on the loss factor. Gou et al. [17] performed a numerical simulation to study the stochastic dynamic behavior of a magnetorheological elastomer sandwich plate. The study showed that the magnetorheological elastomer sandwich plate has a nonlinear dynamic behavior, including stochastic bifurcations. Rokn-Abadi et al. [18] studied the effects of using magnetorheological materials on the stability of a sandwich beam. They showed that the stability of the beam is affected differently depending on the thickness of the central layer as well as the edge conditions. The increase in the intensity of the magnetic field having a strong effect on short lengths for simply supported beams, on the other hand, the intensity of the magnetic field having a strong effect on long lengths for cantilever beams. Rajpal et al. [19] proposed a new technique to integrate a magnetorheological elastomer in passive systems. This technique shows that smart materials can be integrated without using adhesive products. The results of the experiment showed that the MRE sandwich beams perform better in isolating vibrations at the first natural frequency or at lower frequencies. Houshangi et al. [20] analyzed the characteristics of a conical sandwich shell with an MRE core. They evaluated their potential in aeronautical applications. The results showed that the magnetic field density can impact the critical speed, and the use of MRE cores of different thicknesses can also affect the critical speed of these sandwich shells. Li et al. [21] proposed a model to better describe the nonlinear phenomena that occur in the MRE structure when subjected to complex excitation loads. Tests were performed on the MRE structures to study the impact of vibrational excitation energy and the effect of the magnetic field on the nonlinear vibrational characteristics. Experimental results show the reliability of the developed model to predict and evaluate nonlinear dynamic parameters on smart sandwich structures. Kobzili et al. [22] experimentally and numerically studied the effect of an off-axis magnetorheological elastomer of anisotropy on the static and vibratory behavior of a sandwich plate. The results obtained by the two methods are compared. These new structures could open up opportunities in various fields of aeronautics, aerospace, mechanics and civil engineering. Li et al. [23] studied analytically and numerically the skin effect in the case of the bending of sandwich plates, in which the two skins are much more rigid than the honeycomb core. An analytic homogenization method, using series of trigonometric functions, has been proposed to study the influence of the of the honeycomb height on the elastic properties, and the upper and lower bounds of the equivalent elastic moduli. Arani et al. [24] have made an analysis of the instability of MRE sandwich plates with axial displacement. A mathematical modeling of the plate is carried out using the first-order shear deformation theory (FSDT). The study investigates the effects of different parameters on plate instability, such as magnetic field intensity, MR core thickness, particle mass fraction, and boundary conditions and geometric parameters of the plate. The objective is to determine the critical speed at which instability occurs in the plate. The experimental tests carried out by Eloy et al. [25] have shown that the use of an MRE-filled honeycomb core material with carbon fiber/epoxy skins, combined with the application of a magnetic field, can reduce the natural first frequency of the sandwich beam, which contributes to the suppression of vibrations. In addition, an increase in magnetic field intensity resulted in a proportional reduction in vibration amplitude. This approach offers the possibility of modifying the modal parameters of the structure without requiring major modifications of the mass, the geometry or the material of the structure. Fadaee et al. [26] investigated the effects of rotational speed and carbon nanotube reinforcements on the vibration suppression ability of a carbon nanotube-reinforced composite sandwich beam with a magnetorheological core layer. Hamilton's principle and the quadratic difference method (DQM) were used to solve the equations of motion. The results obtained showed an increase in the angular velocity, in particular for values greater than 400 rpm, the latter leading to an increase in the natural frequencies and a reduction in the loss factors. Bastola et al. [27] have made a synthesis and a comprehensive overview of the magneto-mechanical characterizations of MRE as well as a brief coverage of MRE materials and their fabrication methods.

Moreno-Mateos et al. [28] presented an alternative solution based on hard magnetic MRE to provide stiffening responses that can be maintained over time without the need to maintain the external magnetic field enabled by manufacturing novel extremely soft hard magnetic MRE (stiffness of the order of 1 kPa). Bastola et al. [29] have provided a complete picture on magnetoactive soft materials (MSMs). They showed fabrication processes, programming and actuation techniques, behaviors, experimental characterizations, and device-related achievements with current state of the art and future perspectives. Lucarini et al. [30] gave an overview of the state of the art of magneto-active polymers (MAPs), they presented current methods of synthesis, experimental characterization, different computational modeling approaches across scales, and a detailed presentation of their current potential applications. Due to recent advances in the design and development of magneto-/electro-responsive polymers (MERPs), Yarali et al. [31] highlighted in this review article current advances in manufacturing of MERPs using various manufacturing methods including 3D/4D printing and conventional techniques. They also summarized the methods used for the characterization of MERPs and discussed their important structure–property relationship. Hou et al. [32] modeled the damping and vibrations in sectoral and annular plates made of magnetorheological elastomer (MRE) reinforced with glass fibers. The viscoelastic properties of the MRE are described using Maxwell's generalized constitutive law. The effective mechanical properties of the MRE composite (MREC) are determined using a modified version of Voigt's micromechanical rule and Halpin–Tsai's rule. To define the displacement field of the plate, a higher order hyperbolic shear deformation approach is used, and the quadrature approach (GDQ) is exploited. The effects of the composite and the geometry and properties of the structure on the natural frequencies and the modal loss factors of the structure were examined.

The work done by Navazi et al. [33] is focused on the study of the dynamic characteristics of a rotating MRE in a sandwich beam with double taper ratio. The dynamic modeling of the conical beam in rotation is carried out and is made by the energy method. The results indicate that the magnetic field, the width of the beam, the rotational speed and the tuning angle adjusted and increased the natural frequency of the system. Li et al. [34] proposed a nonlinear analytical model to study the effect of the magnetic field temperature on the vibration behavior of a composite plate made of MRE. The results obtained showed that by the application of an internal magnetic field the capacity of the structure for the suppression of vibrations was improved significantly, of the order of 42% to 65%.

The modal analysis of a sandwich composite plate with a honeycomb core was studied by Kumar et al. [35] The sandwich composite plate is modeled using the Ansys APDL software. To characterize the efficiency of the sandwich composite plates with honeycomb core, several parametric investigations were carried out to determine the values of the eigenfrequencies and the mode shapes of the composite sandwich plates using the block Lanczos scheme. The results suggest that the thickness of the face sheet and the material of the core have an impact on the values of the natural frequencies and the mode shapes of the sandwich composite plates. Şakar et al. [36] in this study free vibration analysis of aluminum honeycomb sandwich structures were carried out experimentally and numerically. The natural frequencies and mode shapes of sandwich structures fabricated with different configurations for clamped-free boundary condition were determined. The effects of lower and upper face sheet thickness, the core material thickness, cell diameter, cell angle and foil thickness on the vibration characteristics were examined. Tourab et al. [37] experimentally studied the thermal effect of the magneto-mechanical behavior of elastomer; the latter is infilled with 25% of ferromagnetic particles of micrometric size; developed under the action of a magnetic field. The characterization of the rheological properties and the interaction between the micron size ferromagnetic particles as a function of the intensity of the magnetic field has been studied under the effect of different temperatures. Nayak et al. [38] studied the dynamic stability of a rotating three layered symmetric sandwich beam with a magnetorheological elastomer (MRE) core and conductive skins subjected to axial periodic loads using the finite element method (FEM). The instability regions of the sandwich beam for the principal parametric resonance case were determined using the harmonic balance method. The effects of applied magnetic field, rotation speed, setting angle, hub radius, static load and dynamic load on the dynamic characteristics and instability regions of the sandwich beam were investigated.

In this work, experimental analysis and numerical simulation, of the behavior of hybrid sandwich structures in magnetorheological elastomer honeycomb in bending, were made in order to improve the mechanical resistance and the damping simultaneously.

2 Analytical homogenization model of the bending honeycomb

For a honeycomb core stressed in bending (Fig. 1, 1/8 VER of the honeycomb), the right side (BDFH) is in compression, the left side (ACEG) is on the middle surface of the core and therefore is not subject to any tension or compression. In addition to the displacements imposed by the skins, there are additional displacements (indicated by the dotted lines in Fig. 1) due to stress redistribution.

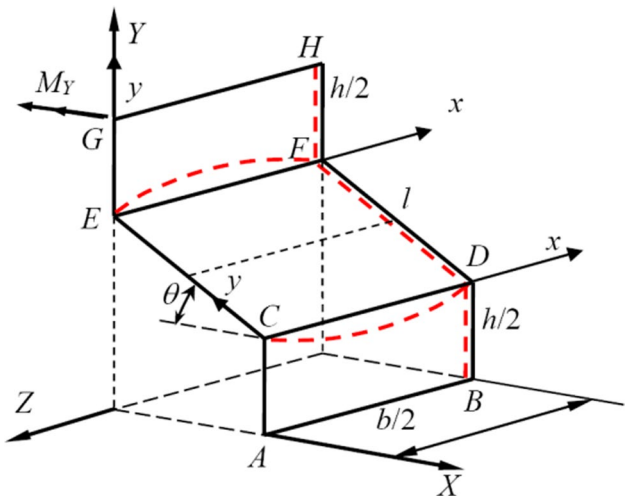

Fig. 1 Additional displacements due to redistribution of bending stresses

In practice, the height of the honeycomb core is neither very small nor very large. The increase in height has a great influence on the redistribution of the stresses between the walls of the honeycomb inducing a notable reduction in the elastic moduli.

2.1 Fields of additional displacements and strains on the vertical wall

The field of additional displacements due to the redistribution of the following stresses is proposed to satisfy the boundary conditions [23].

$$u_h = a_1\frac{2x}{b} + a_2\frac{4x^2}{b^2} \tag{1}$$

$$v_h = \sum_{i=1}^{N}\sum_{j=1}^{N} a_k \sin\frac{m\pi x}{b} + \cos\frac{n\pi y}{h}(m = 2i, n = 2j-1, k = (i-1)N + j + 2) \tag{2}$$

By including the basic deformation imposed by the skins $\varepsilon_Y = -\kappa_Y x$, the deformations in the local coordinate system xy can be defined as follows:

$$u_{xh} = \frac{\partial u}{\partial x} = a_1\frac{2}{b} + a_2\frac{8x}{b^2} \tag{3}$$

$$\varepsilon_{yh} = \varepsilon_Y + \frac{\partial v_h}{\partial y} = -\kappa_Y x - \sum_{i=1}^{N}\sum_{j=1}^{N} a_k\frac{n\pi}{h}\sin\frac{m\pi x}{b} + \sin\frac{n\pi y}{h} \tag{4}$$

$$\gamma_{xyh} = \frac{\partial u}{\partial y} + \frac{\partial v_h}{\partial x} = \sum_{i=1}^{N}\sum_{j=1}^{N} a_k\frac{m\pi}{b}\cos\frac{m\pi x}{b} + \cos\frac{n\pi y}{h} \tag{5}$$

2.2 Fields of additional displacements and strains on the inclined wall

On the inclined wall, the field of additional displacements and the field of deformations are defined in the local coordinate system in the following way (u_l and ε_{xl} are the same as those in the vertical wall) [23]:

$$u_l = a_1\frac{2x}{b} + a_2\frac{4x^2}{b^2} \tag{6}$$

$$v_l = -\sin\theta\sum_{i=1}^{N}\sum_{j=1}^{N} a_k \sin\frac{m\pi x}{b} + \cos\frac{n\pi y}{l}(m = 2i, n = 2j-1, k = (i-1)N + j + 2) \tag{7}$$

$$u_{xh} = \frac{\partial u}{\partial x} = a_1\frac{2}{b} + a_2\frac{8x}{b^2} \tag{8}$$

$$\varepsilon_{yh} = \varepsilon_l + \frac{\partial v_l}{\partial y} = -\kappa_l x + \sin\theta\sum_{i=1}^{N}\sum_{j=1}^{N} a_k\frac{n\pi}{l}\sin\frac{m\pi x}{b} + \sin\frac{n\pi y}{l} \tag{9}$$

$$\gamma_{xyl} = \frac{\partial u_l}{\partial y} + \frac{\partial v_l}{\partial x} = -\sin\theta\sum_{i=1}^{N}\sum_{j=1}^{N} a_k\frac{m\pi}{b}\cos\frac{m\pi x}{b} + \cos\frac{n\pi y}{l} \tag{10}$$

The internal strain energy in the 1/8 REV of the honeycomb is then calculated by:

$$U_{\text{int}} = t_1 \int_0^{b/2}\int_0^{h/2} \left(\frac{E}{1-\nu^2}\left(\varepsilon_x^2 + \varepsilon_{yh}^2 + 2\nu\varepsilon_x\varepsilon_{yh}\right) + G\gamma_{xyh}^2\right)\mathrm{d}y\mathrm{d}x + t_2 \int_0^{b/2}\int_0^{l/2} \left(\frac{E}{1-\nu^2}\left(\varepsilon_x^2 + \varepsilon_{yl}^2 + 2\nu\varepsilon_x\varepsilon_{yl}\right) + G\gamma_{xyl}^2\right)\mathrm{d}y\mathrm{d}x \tag{11}$$

Equations (3), (4), (5), (8), (9), (10) and (11) give:

$$\begin{aligned} U_{\text{int}} = \frac{1}{1-\nu^2}\Bigg\{ & \frac{t_1h+t_2l}{b}\left(a_1^2 + 2a_1a_2 + \frac{3}{4}a_2^2\right) + b^3\frac{t_1h\kappa_Y^2 + t_2l\kappa_l^2}{48} \\ & - \left(t_1\kappa_Y - t_2\kappa_l\sin\theta\right)b^2\sum_{i=1}^{N}\sum_{j=1}^{N}\frac{1}{m\pi}\cos\frac{m\pi}{2}a_k \\ & + b\left(\frac{t_1}{h} + \frac{t_2}{l}\sin^2\theta\right)b^2\sum_{i=1}^{N}\sum_{j=1}^{N}\frac{n^2\pi^2}{16}a_k^2 - 2\nu b\frac{t_1h\kappa_Y + t_2l\kappa_l}{8}a_1 \\ & - 2\nu b\frac{t_1h\kappa_Y + t_2l\kappa_l}{6}a_2 + \frac{1-\nu}{2}\left(\frac{t_1h - t_2l\sin^2\theta}{b}\right)b^2\sum_{i=1}^{N}\sum_{j=1}^{N}\frac{m^2\pi^2}{16}a_k^2 \\ & - \nu\left(t_1 - t_2\sin\theta\right)\left[a_1\sum_{i=1}^{N}\sum_{j=1}^{N}\frac{4}{m\pi}\left(1-\cos\frac{m\pi}{2}\right) - a_2\sum_{i=1}^{N}\sum_{j=1}^{N}\frac{8}{m\pi}\cos\frac{m\pi}{2}\right]a_k\Bigg\} \end{aligned} \tag{12}$$

The minimization of the internal strain energy leads to a system of linear equations to calculate the unknown parameters a_1, a_2 and a_k:

$$\begin{cases} \frac{\partial U_{\text{int}}}{\partial a_1} = 0 \\ \frac{\partial U_{\text{int}}}{\partial a_2} = 0 \\ \frac{\partial U_{\text{int}}}{\partial a_k} = 0 \end{cases} \tag{13}$$

The above equations give:

$$\begin{cases} \frac{t_1h+t_2l}{b}\left(a_1 + a_2\right) - \frac{2\nu}{\pi}\left(t_1 - t_2\sin\theta\right)\sum_{i=1}^{N}\sum_{j=1}^{N}\frac{1}{m}\left(1-\cos\frac{m\pi}{2}\right)a_k = \frac{\nu b}{8}\left(t_1h\kappa_Y + t_2l\kappa_l\right) \\ \frac{t_1h+t_2l}{b}\left(a_1 + \frac{4}{3}a_2\right) + \frac{4\nu}{\pi}\left(t_1 - t_2\sin\theta\right)\sum_{i=1}^{N}\sum_{j=1}^{N}\frac{1}{m}\cos\frac{m\pi}{2}a_k = \frac{\nu b}{6}\left(t_1h\kappa_Y + t_2l\kappa_l\right) \\ -\frac{4\nu}{b}\left(t_1 - t_2\sin\theta\right)\left[a_1\left(1-\cos\frac{m\pi}{2}\right) - 2a_2\cos\frac{m\pi}{2}\right] + \frac{n\pi^3}{8}\left[\left(\frac{t_1}{h} - \frac{t_2}{h}\sin^2\theta\right)n^2 + \frac{1-\nu}{2b^2}\left(t_1h + t_2l\sin^2\theta\right)m^2\right]a_k \\ = \left(t_1\kappa_Y - t_2\kappa_l\sin\theta\right)b\cos\frac{m\pi}{2} \end{cases} \tag{14}$$

The unknown parameters a_1, a_2 and a_k can be obtained by solving the above system numerically. We can also obtain a_1, a_2 and a_k in Eq. (14) semi-analytically (see Appendix).

The strain energy of the top and bottom skins of the MRE composite sandwich plates can be expressed as follows [37]:

$$U_1 = \int_0^a\int_0^b \left\{D_{111}\left(\frac{\partial^2 w_1}{\partial x^2}\right)^2 + 2D_{112}\left(\frac{\partial^2 w_1}{\partial x^2}\frac{\partial^2 w_1}{\partial y^2}\right) + D_{122}\left(\frac{\partial^2 w_1}{\partial y^2}\right)^2 + 4D_{166}\left(\frac{\partial^2 w_1}{\partial x\partial y}\right)^2\right\}\mathrm{d}x\mathrm{d}y \tag{15}$$

$$U_3 = \int_0^a\int_0^b \left\{D_{311}\left(\frac{\partial^2 w_3}{\partial x^2}\right)^2 + 2D_{312}\left(\frac{\partial^2 w_3}{\partial x^2}\frac{\partial^2 w_3}{\partial y^2}\right) + D_{322}\left(\frac{\partial^2 w_3}{\partial y^2}\right)^2 + 4D_{366}\left(\frac{\partial^2 w_3}{\partial x\partial y}\right)^2\right\}\mathrm{d}x\mathrm{d}y \tag{16}$$

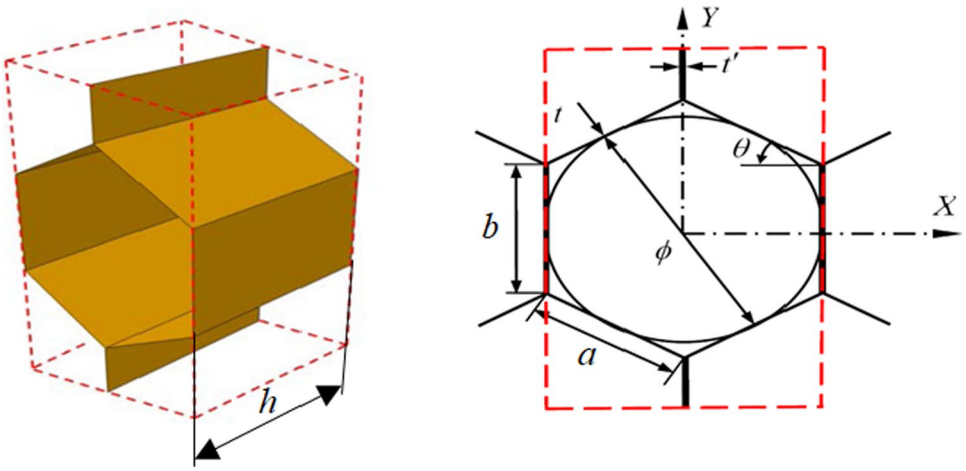

Fig. 2 Representative elementary volume and geometry of a honeycomb

Table 1 Geometric parameters and mechanical properties of the honeycomb cell material

ϕ(mm)	a(mm)	b(mm)	h(mm)	t(mm)	t'(mm)	θ
6.35	3,66	3,66	5	1	2	30°
	$\rho_h(Kg/m^3)$			$E_h(MPa)$		ν_h
	2800			72,000		0,33

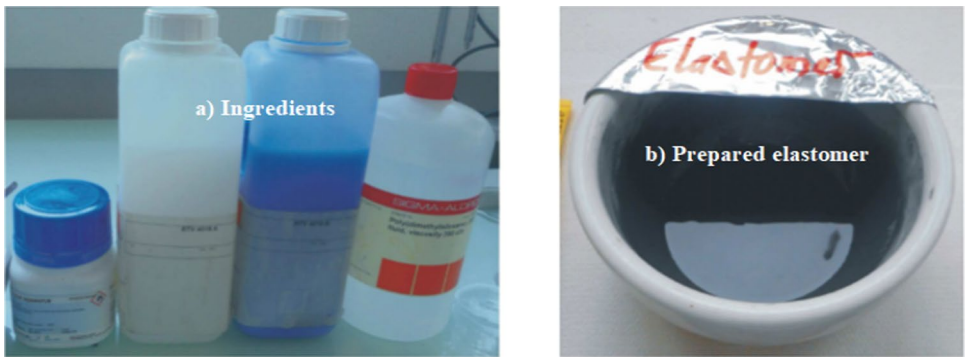

Fig. 3 **a** Ingredients of the elastomer, **b** prepared elastomer

Table 2 Constituents of the magnetorheological elastomer

$m_{\text{huile de silicone}}$ (g)	$m_{RTV(A)}$ (g)	$m_{RTV(B)}$ (g)	m_{Fe}(g)
1.064 g	1.0385 g	0.104	7.559

The strain energy of the elastomeric core is given as follows

$$U_2 = \frac{2d}{h_2}\int_0^a\int_0^b G_2(1+i\eta)\left(\frac{\partial w}{\partial x}\right)^2 dxdy \tag{17}$$

$$d = \frac{1}{2}(h_1 + 2h_2 + h_3)$$

The total strain energy of the sandwich plate (U) can be expressed as follows

Fig. 4 Lower part of the mold

Fig. 5 Elastomer injected into the mold

Fig. 6 Aluminum top skin

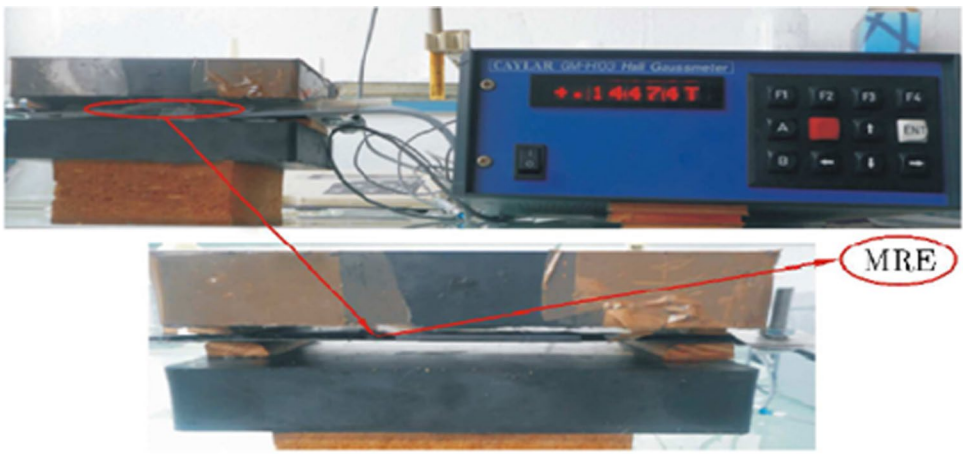

Fig. 7 Device for crosslinking the elastomer infilled with 30% iron particles

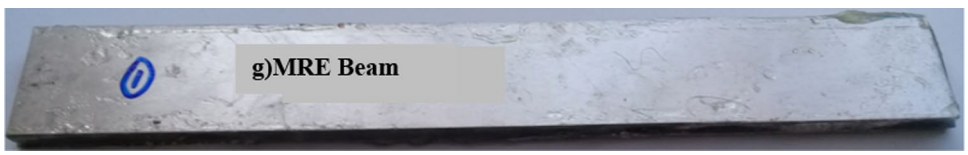

Fig. 8 Magnetorheological elastomer (MRE) beam

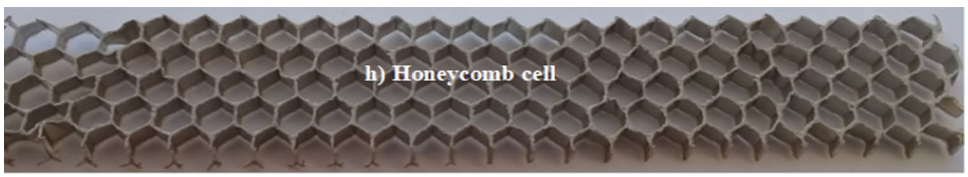

Fig. 9 Honeycomb cells

$$U = U_{1,3} + U_2 + U_{\text{Honey}} \tag{18}$$

$$D_{11} = D_{22} = D, D_{12} = \nu D, D_{66} = \left(\frac{1-\nu}{2}\right) D$$

where $D_i = D = EI$ $(i = 1, 3)$ is the bending stiffness of the skins, w is the transverse displacement of the plate, G_2 and h_2 are, respectively, the shear modulus and the thickness of the elastomer, respectively.

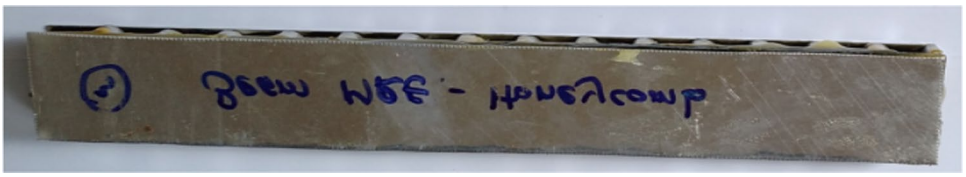

Fig. 10 Technique for manufacturing a hybrid MRE-Honeycomb beam (one layer of honeycomb)

Fig. 11 Fabrication technique of a hybrid MRE-honeycomb beam (two layers of honeycomb)

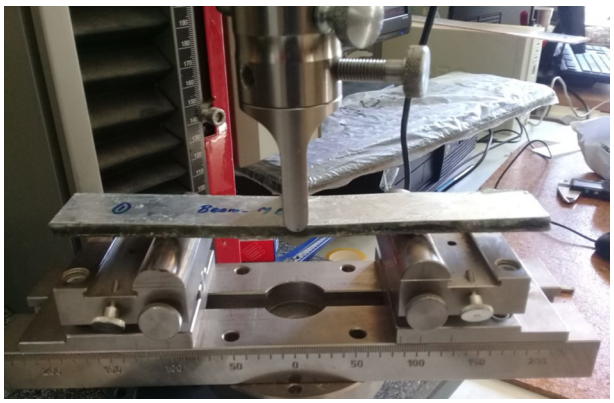

Fig. 12 Three-point bending test

3 Experimental study

3.1 Elaboration and geometry of honeycomb

The chosen honeycomb geometry is based on regular hexagonal cells Fig. 2.

The geometric parameters and mechanical properties of the aluminum honeycomb cell are presented in Table 1.

3.2 Fabrication of the magnetorheological elastomer and sandwich hybrid beam

The elastomer and the magnetorheological sandwich hybrid beam are prepared according to the following steps.

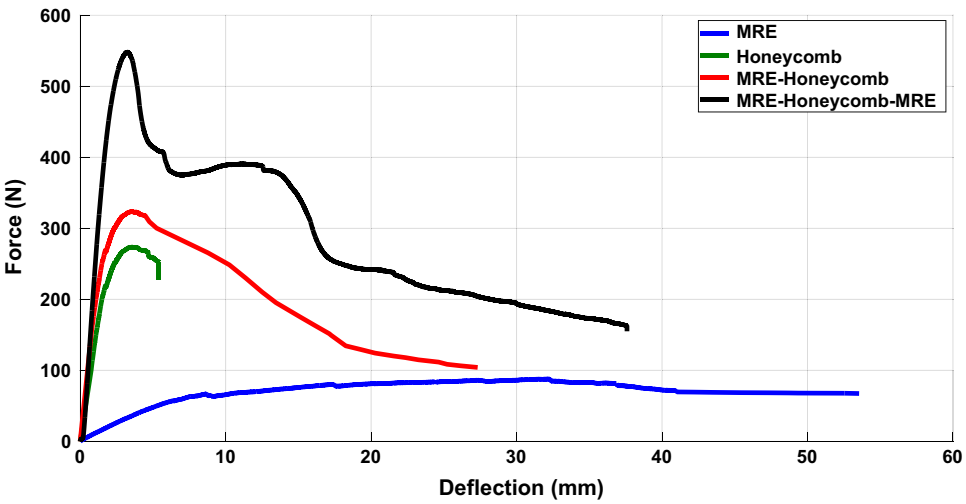

Fig. 13 3-point bending of four elaborated specimens

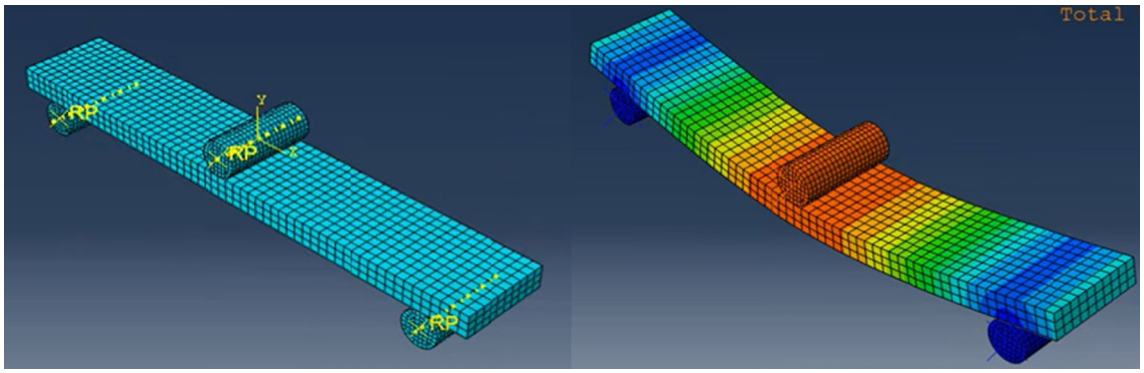

Fig. 14 Three-point bending of structure modeled by Abaqus and boundary conditions

1. The silicone oil and the RTV141A polymer (Fig. 3) were manually mixed in a container for 10 min to obtain a well-homogenized elastomer gel.
2. A quantity of this gel obtained by silicone and RTV141A is mixed for 30 min with a quantity of iron particles until a homogeneous paste is obtained. By this process, an elastomer infilled with 30% ferromagnetic particles is produced (Fig. 3). @@@ In our work, we have chosen an ideal percentage of filling of 30%, to obtain the best properties of the MRE. The complex modulus and loss factor of MRE are determined under a magnetic field intensity of 0.1 T. The experimental results show that the complex modulus of the MRE increases with the increase in the magnetic field intensity which will directly influence the rigidity of the plates elaborated in MRE. The constituents in mass fraction of the elastomer produced are given in Table 2.
3. A mold (lower aluminum skin + rubber gasket) of the shape of the beam was made (Fig. 4).
4. The elastomer paste obtained previously (Fig. 3) was injected into a rectangular mold, of 30 cm long, 3 cm width and 2 mm thick (Fig. 4). This step, represented in Fig. 5, represents the first part of the beam.
5. An upper aluminum skin given in Fig. 6 is glued to the mold filled with the elastomer paste (Fig. 5).
6. By this process, a beam formed of two aluminum skins and an elastomer core infilled with 30% ferromagnetic particles is produced. The latter is subjected to a magnetic field as shown in Fig. 7.
7. After this last step, we have manufactured a magnetorheological elastomer beam (Fig. 8).
8. The honeycomb cells given in Fig. 9 are glued on the upper or lower skin of the MRE beam (Fig. 9).
9. Two MRE elastomer beams are glued on either side of a layer of honeycomb cells to form a hybrid MRE-honeycomb beam with one honeycomb layer (Fig. 10).

Table 3 Properties of the aluminum skins

$\rho_s(Kg/m^3)$	E_s(MPa)	v_s	h_s(mm)	L_s(mm)	b_s(mm)
2800	72,000	0.33	1	200	30

Table 4 Properties of the MRE

$\rho_{MRE}(Kg/m^3)$	E_{MRE}(MPa)	v_{MRE}	h_{MRE}(mm)	L_{MRE}(mm)	b_{MRE}(mm)
1100	1.7	0.45	2	200	30

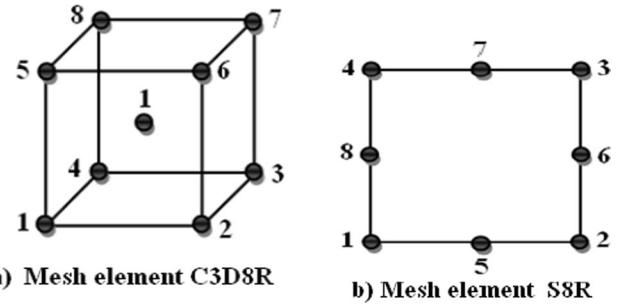

Fig. 15 Types of mesh elements used

And by the same process, we can obtain a hybrid MRE-honeycomb beam with two layers of honeycomb (Fig. 11).

Figure 2 Fabrication technique used for the development of the MRE-honeycomb hybrid structure.

The hybrid sandwich beams developed previously (Fig. 2) are characterized by the three-point bending test. This test is carried out on Instron 8561 universal testing machine equipped with a 10 kN sensor. The feed rate is 2 mm/min. Data acquisition is performed using software that give displacement as a function of force. Figure 12 represents the three-point bending

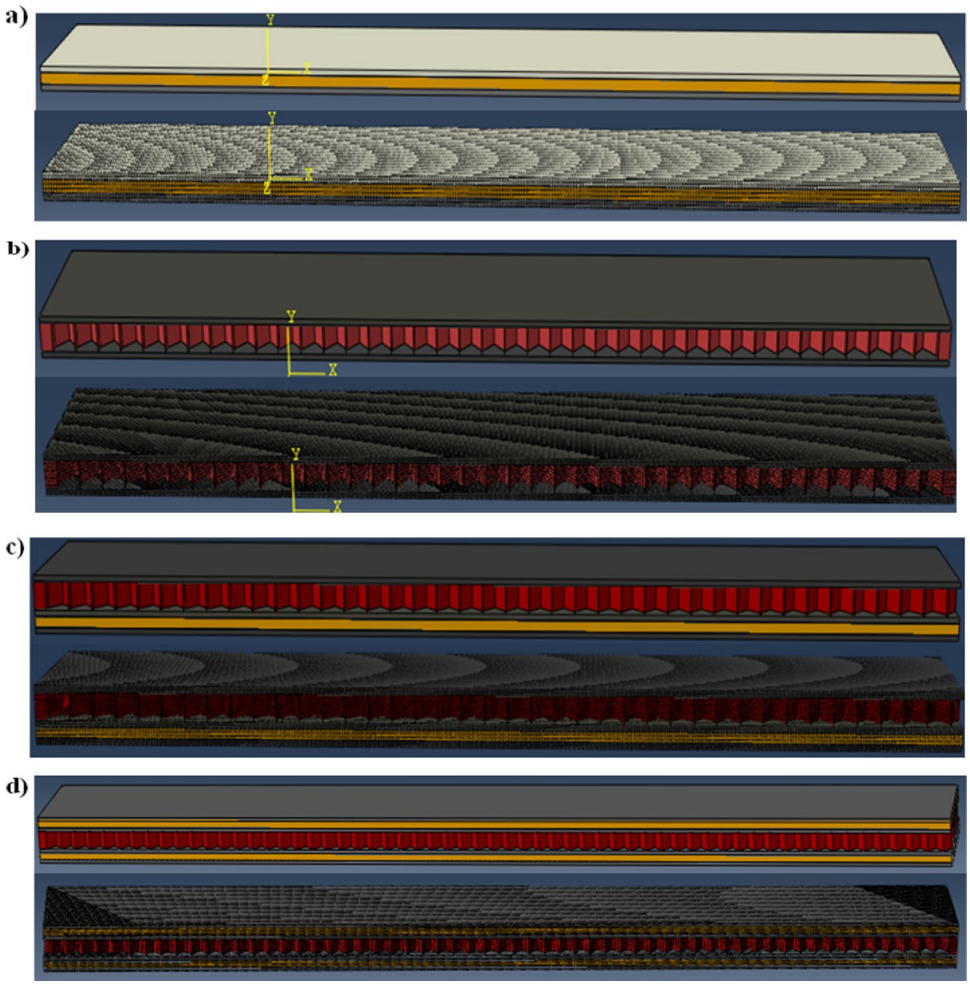

Fig. 16 Different beams, **(a)** MRE **(b)** honeycomb **(c)** MRE-honeycomb **(d)** MRE-honeycomb-MRE

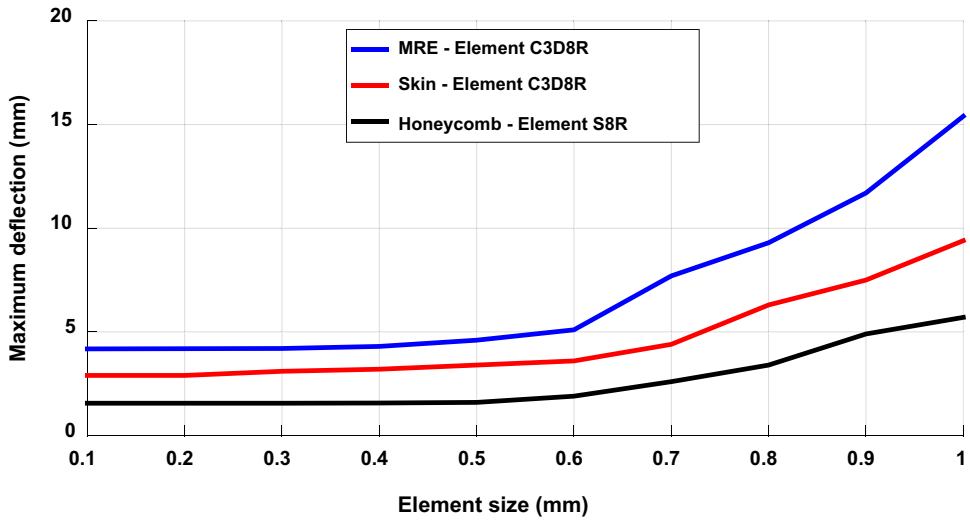

Fig. 17 Mesh convergence

test. The ASTM D7249 and ASTM D7250 standards provide guidelines for the parameters to use for the test (Fig. 13).

3.3 Analysis and discussion

The results of this set of experimental tests are presented in the form of force–deflection curves for each specimen

Table5 Boundary conditions

Degree of freedom	Essential	Natural
Transverse	w_y	Shear force
Rotation	θ_z	Moment
Slip	Δ_i	Normal fore

Table 6 Boundary conditions in displacement and rotation

simple—simple boundary condition	$w = 0$
	$\frac{\partial^2 w}{\partial x^2} = 0$

(Fig. 14).

Figure 14 shows the three-point bending test performed for different engineered beams (Instron 8561 universal testing machine). It is noted that the honeycomb specimen reaches a rapid rupture with a deflection of 5.4 mm, as well as this specimen supports a maximum force of 268 N. On the other hand, the MRE specimen has a deflection value of 53.5 mm and will not reach its breaking point with a maximum supported force less than 100 N. It is also observed, for the two hybrid specimens in magnetorheological elastomer and honeycomb, that the breaking point increases with a considerable increase in the maximum force applied especially for the case of the MRE-honeycomb-MRE specimen. We have practically the same deflection (3.6 mm for the MRE single layer beam and 3.25 mm for the MRE double layer beam) with a different maximum force (323.6 N for the MRE single layer beam and 548.2 N for the MRE double layer beam).

In conclusion of all the static tests carried out on the four different types of elaborated specimens (Fig. 4), it is found that the hybrid specimens are the most reliable in terms of rigidity and damping and have a better mechanical resistance due to the layer of honeycomb structure and good fracture toughness due to the MRE layer (strength until the MRE layer breaks).

4 Numerical simulation

To evaluate the accuracy and efficiency of our finite element model, we perform three types of calculation: (1) modeling of the honeycomb core by Abaqus shell elements with a very fine mesh to describe the complex geometry of the honeycomb; (2) modeling of the MRE by solid elements of Abaqus with viscoelastic material properties; and (3) modeling of the skins by solid elements of Abaqus with the elastic solid properties.

To validate the results of our simulation, we consider the same material and geometric data of MRE, honeycomb and skins used in the experimental part.

The mechanical characteristics of the magnetorheological elastomer were measured experimentally in the Condensed Matter Physics Laboratory of the University of Côte d'Azur—France.

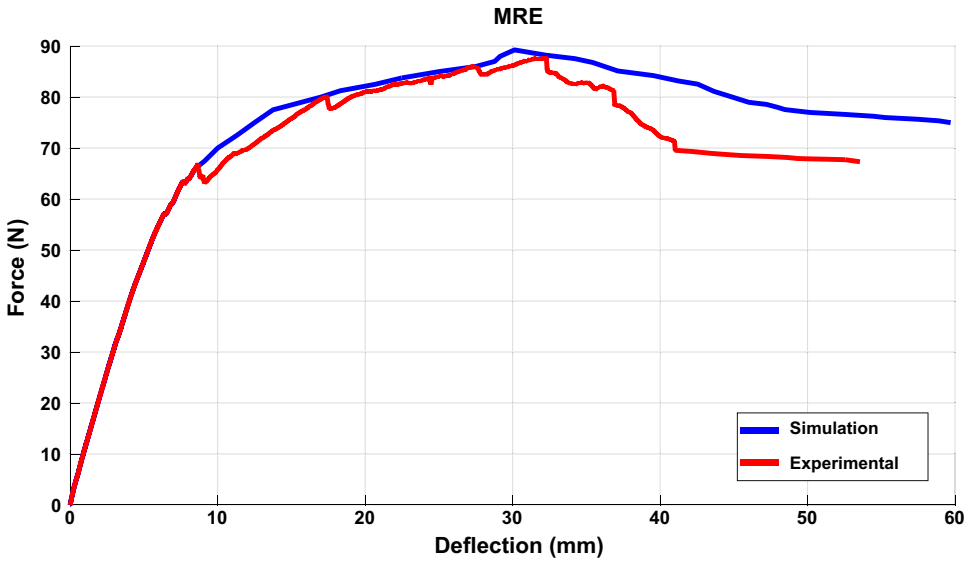

Fig. 18 Comparison between the experimental and numerical results of the specimen in MRE

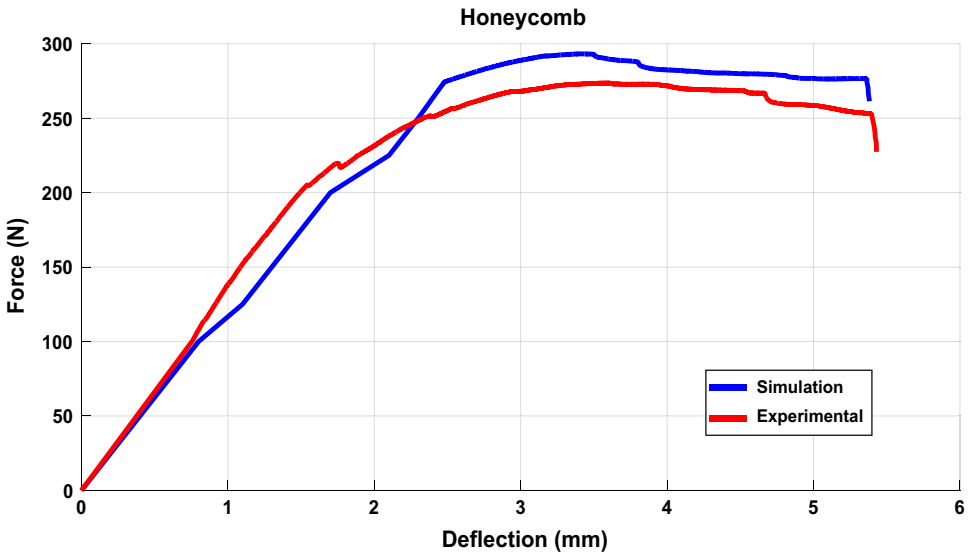

Fig. 19 Comparison between the experimental and numerical results of the honeycomb specimen

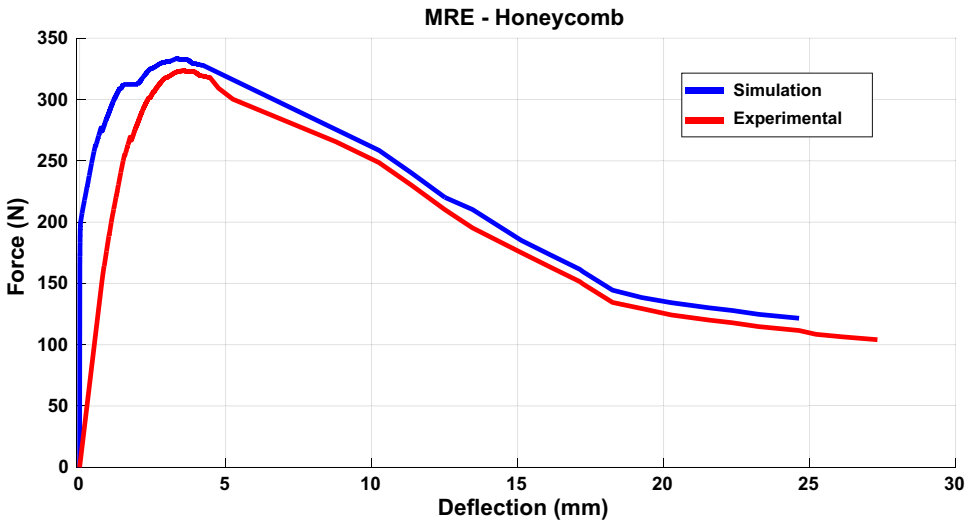

Fig. 20 Comparison between the experimental and numerical results of the MRE-honeycomb specimen

The mechanical and geometric characteristics of the skins are given in Tables 3 and 4.

The mechanical and geometric characteristics of the skins are given in Table 3.

The mechanical and geometric characteristics of the honeycomb are given in Table 1.

In the numerical part of this present work, we studied a similar case with the experimental part, that is to say we studied the case of a three-point bending of a beam resting on two simple supports (UX=UY=UZ=URY=URZ = 0) and subjected to a load in the middle (Fig. 15).

To model the bending behavior of the various beams studied, a second-order C3D8R 3D solid element is used to discretize the skin and the core in MRE (Fig. 15). A first-order S8R shell element is used to discretize the honeycomb part (Fig. 15).

The various simulated beams and their mesh are given in Fig. 16a–d.

The evolution of the maximum deflection according to the mesh size is shown in Fig. 17. The results of the successive calculations are converged with a mesh size of 0.2 mm in length of the MRE and the aluminum skin. Convergence is obtained with a mesh size of 0.4 mm honeycomb length. We also note that the sensitivity study highlights the increase in the maximum deflection with the decrease in the size of the elements. We can then say that the deflection has converged in the case of the MRE and the aluminum skin for an element value of $0.2 \times 0.2 \times 0.2$ m^3 and is converged in the case

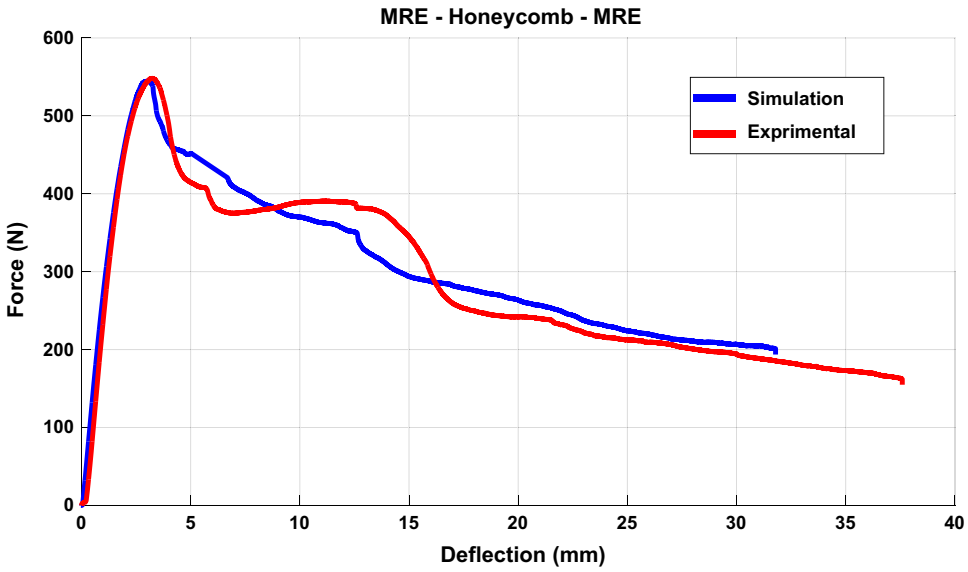

Fig. 21 Comparison between the experimental and numerical results of the MRE-honeycomb-MRE specimen

Table 7 Comparison between experimental and numerical results in terms of maximum applied force and deflection

Beam	Maximum applied force (N)			Deflection (mm)		
	Experimental	numerical	Δ%	Experimental	numerical	Δ%
MRE	87	89	**2.3**	31.47	30.40	**3.5**
Honeycomb	274	279	**1.8**	03.56	3.65	**2.5**
MRE-Hony	323	334	**3.4**	03.80	03.73	**1.9**
MRE-Hony-MRE	548	546	**0.4**	03.17	03.21	**1.6**

Bold means the difference between experimental and numerical results

of honeycomb for an element value of 0.4×0.4 m^2, these element sizes will be used in our work.

The essential, natural boundary conditions and the displacement and rotation boundary conditions are summarized in Tables 5 and 6.

4.1 Interpretation and validation of results

The finite element numerical analysis of the static behavior in three-point bending of the MRE-honeycomb hybrid sandwich beams (Fig. 15) was carried out by simulation using the Abaqus calculation code. Each simulation studied was the subject of several tests of 3 to 5 per specimen. The results in the form of transverse force–deflection curves are summarized in Figs. 18, 19, 20 and 21 for each beam model.

Figure 11 presents the results of the three-point bending test carried out on the MRE beam (Fig. 15). It can be seen that this structure has a very high rupture limit of more than 60 mm with a weak maximum applied force of 89 N. Thus, it can be noted that the difference between the two values of the experimental and numerical deflection, for the maximum applied forces of 87 and 89 N, is 3.5% (Table 7). According to Boczkowska et al. [39], MREs are promising, novel materials for a wide range of potential applications. The stiffness of MREs can be increased under an applied magnetic field. Magnetorheological elastomers are used to improve the stiffness and damping of mechanical structures [40].

Figure 12 presents the three-point bending test results performed on the honeycomb beam (Fig. 16). It is observed that this structure has a very short breaking point less than 5.5 mm with a high maximum applied force of 279 N. It can be observed that the difference between the two values of the experimental and numerical deflection, for the maximum applied forces of 279 N. and 274 N, is 2.5% (Table 7). Cell cores offer improvements in bending stiffness capabilities [41]. It can be seen similar results to Fig. 12 in some correlated works, such as Xiao et al. [42], Li et al. [43] and Fu and Sadeghian [44].

Figure 19 presents the three-point bending test results performed on the single-layer MRE-honeycomb beam (Fig. 16). It is noted that this structure has a very high rupture limit more than 27 mm with a high maximum applied force of 334 N. The difference between the two values of the experimental and numerical deflection, for the maximum applied forces of 334 and 323 N, is 1.9% (Table 7).

Figure 15 presents the three-point bending test results performed on the double-layer MRE-honeycomb beam (Fig. 16). It is noted that this structure has a very high

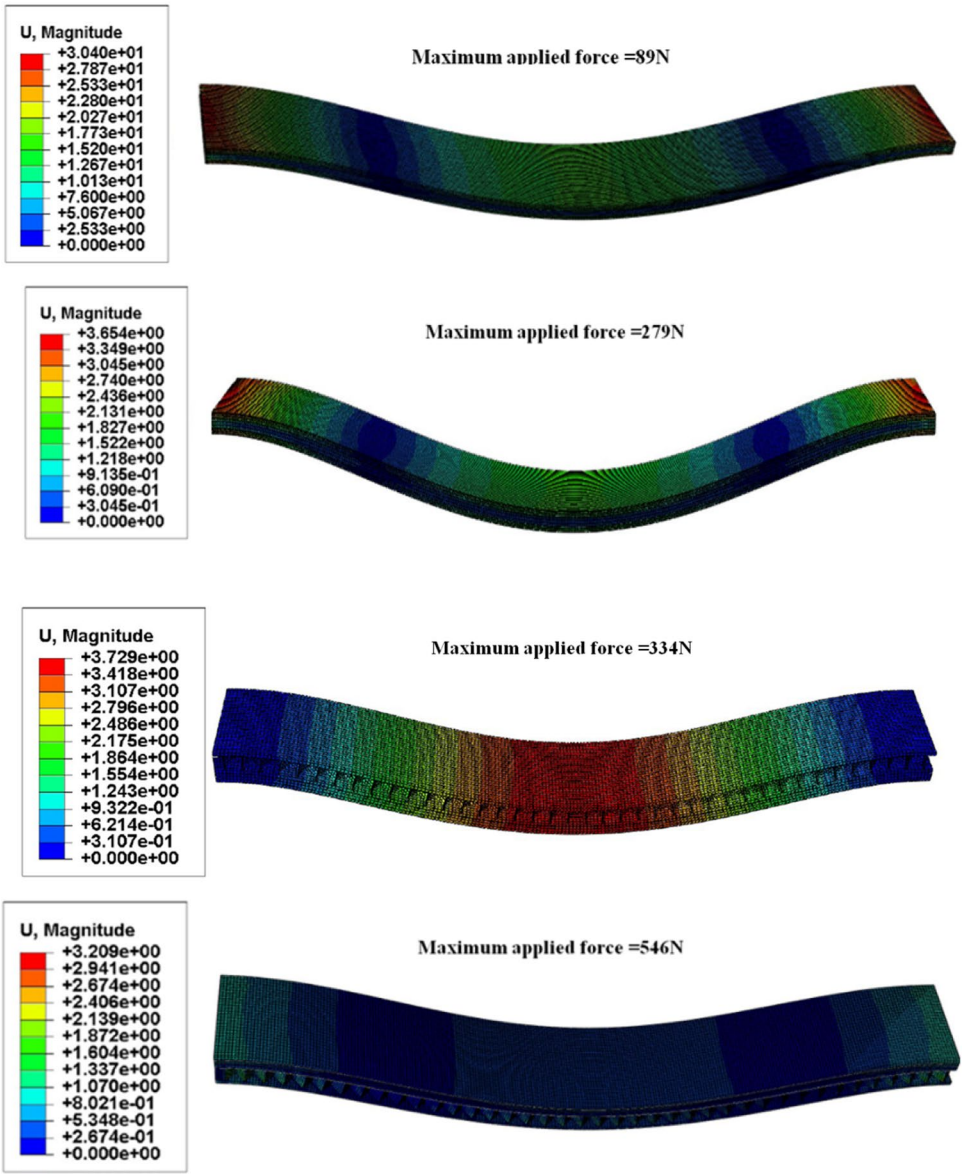

Fig. 22 Mode of deformation of different specimens: **(a)** MRE, **(b)** honeycomb, **(c)** MRE-honeycomb, **(d)** MRE-honeycomb-MRE

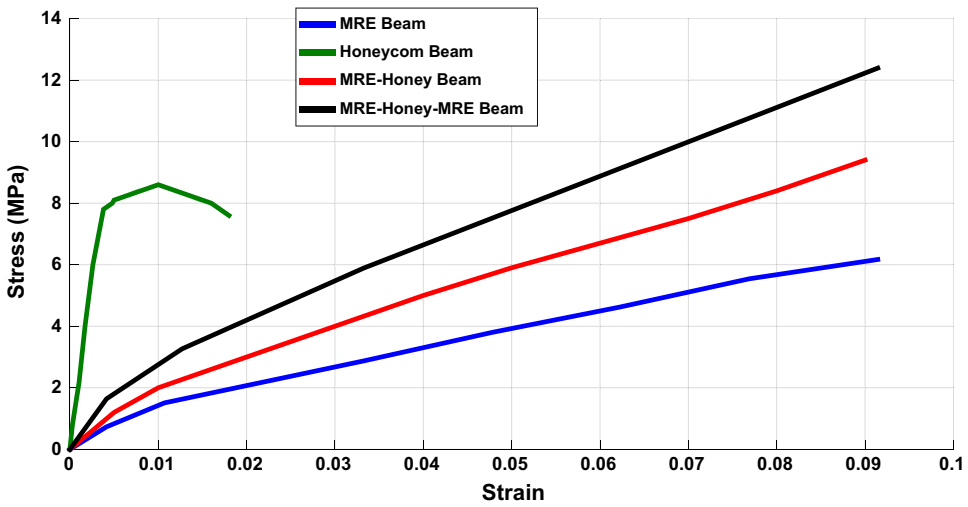

Fig. 23 Stress–strain variation of different cases

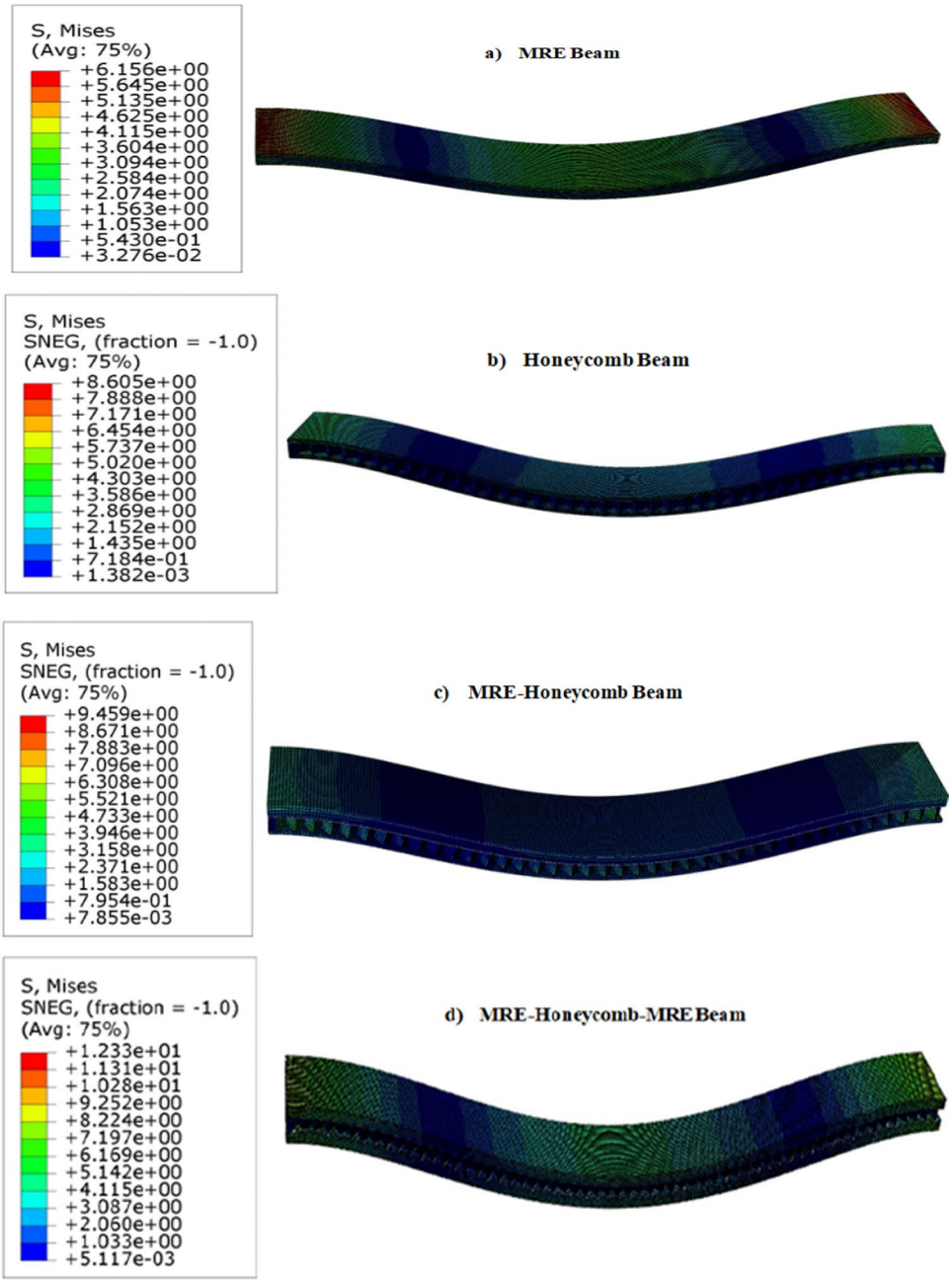

Fig. 24 Modes of deformations for different cases

breaking limit of more than 33 mm with a very high maximum applied force of 546 N. The difference between the two values of the experimental and numerical deflection, for the maximum applied forces of 546 and 548 N, is 1.6% (Table 7).

It is interesting to note that the stiffness and the damping are very important in the case of the MRE-honeycomb beam (Figs. 20 and 21). We also note that the transverse deflection of different specimens as a function of the applied force is very important in the case of beams having a layer of magnetorheological elastomer (Figs. 18, 19, 21). We can quote a work carried out in this direction by Felipe de Souza Eloydans et al. [25]. In this paper, free and forced vibration tests conducted under several magnetic field intensities were performed to evaluate dynamic properties of the sandwich beams with carbon/epoxy composite skins and a honeycomb core filled with magnetorheological elastomer (Fig. 22).

We observe a good agreement between the results obtained by experimental analysis and the numerical results obtained using Abaqus software.

We present in Fig. 16 the deformation of different specimens subjected to different applied forces. It can be seen

that the maximum deflection is located at the center for each beam. The percentage difference between the experimental and numerical results in terms of maximum applied force and deflection is given in Table 7.

In the numerical part of this article, we studied the variation of the stresses according to the strains for each case of beam. Figure 23 shows the curve of this variation in three-point bending test simulated by the Abaqus software, a nonlinear behavior is observed in the case of beams having a magnetorheological elastomer layer, this nonlinear behavior of the elastomers is due to the effect of the magnetic field [30] and it can also be linked to viscoelastic models of the stress–strain function $\sigma(\varepsilon)$ [45, 46]. On the other hand, the honeycomb beam shows a linear behavior of an elastic solid [47]. Therefore, the bending curve (Fig. 23) shows a considerable nonlinear increase in stress as a function of strain for the case of MRE-Honeycomb hybrid beams.

The results of the simulation and the deformation modes are illustrated in Fig. 24.

5 Conclusion

This research work presents a study on the static behavior of hybrid sandwich beams in honeycomb magnetorheological elastomer. The objective is to identify the static behavior in three-point bending of these new structures in smart composite material. The study of the static behavior was made by the two experimental and numerical methods using Abaqus (finite elements software). The mechanical properties of the beam are adjustable by applying a magnetic field intensity of 0.14 T. The resistance of the specimen made of honeycomb core and a layer of magnetorheological elastomer is practically 6 times more rigid compared to the rigidity of the specimen in MRE, with an improvement ratio of 600%; and 2 times stiffer compared to the resistance of the honeycomb specimen; with a 200% improvement ratio. The specimens developed with a honeycomb core and a layer of magnetorheological elastomer have a very high breaking limit; this rupture only occurs after a deflection of 35 mm, i.e., with an increase of 600% compared to the rupture limit of the honeycomb specimen where the latter occurs at a deflection of 5.5 mm. It is found that the elaborate specimens of honeycomb core and a layer of magnetorheological elastomer provide a great possibility to improve the damping capabilities as well.

Appendix

The system of Eqs. (14) is solved semi-analytically and the unknowns of the problem are given as follows:

$$a_1 = \frac{A_{22}B_1 - A_{12}B_2}{A_{11}A_{22} - A_{21}A_{12}}$$

$$a_2 = \frac{A_{11}B_2 - A_{21}B_1}{A_{11}A_{22} - A_{21}A_{12}}$$

$$a_k = \frac{C_1 + C_2 a_1 + C_3 a_2}{D}$$

with:

$$A_{12} = A_{11} = \left(t_1 h + t_2 l\right) - 4\nu^2\left(t_1 - t_2 \sin\theta\right)^2 \sum_{i=1}^{N}\sum_{j=1}^{N} \frac{2}{m^2\pi^2}\left(1 - \cos\frac{m\pi}{2}\right)^2 \frac{1}{\phi_k}$$

$$B_1 = \nu\frac{t_1 h\kappa_Y + t_2 l\kappa_l}{8} b^2 + \nu\left(t_1\kappa_Y - t_2\kappa_l \sin\theta\right)\left(t_1 - t_2\sin\theta\right) \sum_{i=1}^{N}\sum_{j=1}^{N} \frac{2}{m^2\pi^2}\left(1 - \cos\frac{m\pi}{2}\right)\cos\frac{m\pi}{2}\frac{1}{\phi_k} b^2$$

$$A_{21} = \left(t_1 h + t_2 l\right) + 4\nu^2\left(t_1 - t_2\sin\theta\right)^2 \sum_{i=1}^{N} \sum_{j=1}^{N} \frac{4}{m^2\pi^2}\cos\frac{m\pi}{2}\left(1 - \cos\frac{m\pi}{2}\right)\frac{1}{\phi_k}$$

$$A_{22} = \frac{4}{3}\left(t_1 h + t_2 l\right) - 8\nu^2\left(t_1 - t_2\sin\theta\right)^2 \sum_{i=1}^{N}\sum_{j=1}^{N} \frac{4}{m^2\pi^2}\frac{1}{\phi_k}$$

$$B_2 = \nu\frac{t_1 h\kappa_Y + t_2 l\kappa_l}{6} b^2 - \nu\left(t_1 - t_2\sin\theta\right)\left(t_1\kappa_Y - t_2\kappa_l\sin\theta\right) \sum_{i=1}^{N}\sum_{j=1}^{N} \frac{4}{m^2\pi^2}\frac{1}{\phi_k} b^2$$

$$\phi_k = \left(\frac{t_1}{h} + \frac{t_2}{l}\sin^2\theta\right)\frac{n^2\pi^2}{8} + \frac{1-\nu}{2}\frac{1}{b^2}\left(t_1 h - t_2 l\sin^2\theta\right)\frac{m^2\pi^2}{8}$$

$$C_1 = \left(t_1\kappa_Y - t_2\kappa_l\sin\theta\right) b\ \cos\frac{m\pi}{2}$$

$$C_2 = \frac{4\nu}{b}\left(t_1 - t_2\sin\theta\right)\left(1 - \cos\frac{m\pi}{2}\right)$$

$$C_3 = -\frac{8\nu}{b}\cos\frac{m\pi}{2}\left(t_1 - t_2\sin\theta\right)$$

$$D = \frac{n\pi^3}{8}\left[\left(\frac{t_1}{h} + \frac{t_2}{l}\sin^2\theta\right)n^2 + \frac{1-\nu}{2b^2}\left(t_1 h + t_2 l\sin^2\theta\right)m^2\right]$$

Acknowledgements Many thanks to the materials and complex fluids research team of the physics and condensed matter laboratory for their unfailing help, especially Dr. Pavel Kuzhir.

Authors Contributions SA, LG and NC were involved in conceptualization, methodology, formal analysis, and writing–original draft. TD, LK, MM and AN contributed to conceptualization, resources, supervision, and writing–review.

Declarations

Conflict of interest The authors declare no conflict of interest.

References

1. Janbaz M, Googarchin HS (2020) Experimental and numerical analysis on magneto-hyper-viscoelastic constitutive responses of magnetorheological elastomers: a characterization procedure. Mechan Mater 154(5):103712. https://doi.org/10.1016/j.mechmat.2020.103712
2. Dargahi A, Sedaghati R, Rakheja S (2019) On the properties of magnetorheological elastomers in shear mode: Design, fabrication and characterization. Compos B 159:269–283. https://doi.org/10.1016/j.compositesb.2018.09.080
3. Bernat J, Gajewski P, Kołota JA (2023) Marcinkowska, "review of soft actuators controlled with electrical stimuli: IPMC, DEAP, and MRE. Appl Sci 13(3):1651. https://doi.org/10.3390/app13031651
4. Khairi MHA, Noor EEM, Ubaidillah U, Aziz SAA, Mazlan SA, Tarmizi SMA, Nordin NA (2022) Enhancement of magneto-induced modulus by the combination of filler and plasticizer additives-based magnetorheological elastomer. Materials 15(18):6396. https://doi.org/10.3390/ma15186396
5. Bhaktha S, Hegde S, Rao SU (2022) Experimental analysis of viscoelastic properties of room temperature vulcanized silicone based magnetorheological elastomer. Defen Sci J 72(1):98–104. https://doi.org/10.14429/dsj.72.17089
6. Keshav M, Sujatha C (2022) Study of distribution of magnetic field strength in magnetorheological elastomers using artificial neural network. IOP Conf Ser Mater Sci Eng 1258:12039. https://doi.org/10.1088/1757-899X/1258/1/012039
7. Moreno-Mateos MA, Hossain M, Steinmann P, Garcia-Gonzalez D (2022) Hybrid magnetorheological elastomers enable versatile soft actuators. Computat Mater 8:162. https://doi.org/10.1038/s41524-022-00844-1
8. Makarova L, Nadzharyan TA, Alekhina YA, Stepanov GV, Kazimirova EG, Perov NS, Kramarenko EY (2017) Magnetoactive elastomer as an element of a magnetic retina fixator. Smart Mater Struct 26(9):095054. https://doi.org/10.1088/1361-665X/aa82e9
9. Saxena P, Hossain M, Steinmann P (2013) A theory of finite deformation magneto-viscoelasticity. Int J Solids Struct 50(24):3886–3897. https://doi.org/10.1016/j.ijsolstr.2013.07.024
10. Lian C, Lee K-H, Lee C-H (2016) Friction and wear characteristics of magnetorheological elastomer under vibration conditions. Tribol Int 98:292–298. https://doi.org/10.1016/j.triboint.2016.02.037
11. Nedjar A, Aguib S, Djedid T, Nour A, Settet A, Tourab M (2019) Analysis of the dynamic behavior of magnetorheological elastomer composite: elaboration and identification of rheological properties. SILICON 11:1287–1293. https://doi.org/10.1007/s12633-018-9921-1
12. Eloy FS, Gomes GF, Ancelotti AC Jr, Cunha SS Jr, Bombard AJF, Junqueira DM (2019) A numerical-experimental dynamic analysis of composite sandwich beam with magnetorheological elastomer honeycomb core. Compos Struct 209:242–257. https://doi.org/10.1016/j.compstruct.2018.10.041
13. Li H, Wang W, Wang X (2022) Static and dynamic performances of sandwich plates with magnetorheological elastomer elastomer core: theoretical and experimental studies. J Sandw Struct Mater 24(3):362. https://doi.org/10.1177/1099636221105
14. Selvaraj R, Ramamoorthy M (2020) Dynamic analysis of laminated composite sandwich beam containing carbon nanotubes reinforced magnetorheological elastomer. J Sandw Struct Mater 23(5):1784. https://doi.org/10.1177/1099636220905253
15. Liu J, Xie Z, Gao J, Hu Y, Zhao J (2022) Failure characteristics of the active-passive damping in the functionally graded piezoelectric layers-magnetorheological elastomer sandwich structure. Int J Mechan Sci 215:10644. https://doi.org/10.1016/j.ijmecsci.2021.106944
16. Dai Z, Wu S, Habibi M, Ali HE (2023) Application of point interpolation mesh-free method for magneto/electro rheological vibrations of sandwich conical panels. Aerosp Sci Technol 135:108180. https://doi.org/10.1016/j.ast.2023.108180
17. Gou W-J, Zhu Z-W (2023) Nonlinear dynamics of Magnetorheological elastomer sandwich plate under stochastic excitation. J Phys Conf Ser 2430:012024. https://doi.org/10.1088/1742-6596/2430/1/012024
18. Rokn-Abadi M, Yousefi M, Haddadpour H, Sadeghmanesh M (2020) Dynamic stability analysis of a sandwich beam with magnetorheological elastomer core subjected to a follower force. Acta Mech 231:3715–3727. https://doi.org/10.1007/s00707-020-02735-2
19. Rajpal R, Lijesh KP, Gangadharan KV (2018) Experimental investigation of 3D-printed polymer-based MR sandwich beam under discretized magnetic field. J Braz Soc Mechan Sci Eng 40:569. https://doi.org/10.1007/s40430-018-1488-7
20. Houshangi A, Jafari AA, Haghighi SE, Nezami M (2022) Supersonic flutter characteristics of truncated sandwich conical shells with MR core. Thin-Walled Struct. https://doi.org/10.1016/j.tws.2022.108888
21. Li H, Wang X, Dai Z, Xia Y, Ha SK, Wang X, Ren Y, Han Q, Wu H (2023) Magnetic and vibrational amplitude dependences of MRE grid composite sandwich plates. Int J Mechan Sci 24:107978. https://doi.org/10.1016/j.ijmecsci.2022.107978
22. Kobzili L, Aguib S, Chikh N, Djedid T, Meloussi M (2021) Modeling and simulation of the static and vibratory behavior of hybrid composite plate off-axis anisotropic. Compos Struct 273:114297. https://doi.org/10.1016/j.compstruct.2021.114297
23. Li YM, Hoang MP, Abbes B, Abbes F, Guo YQ (2015) Analytical homogenization for stretch and bending of honeycomb sandwich plates with skin and height effects. Compos Struct 120:406–416. https://doi.org/10.1016/j.compstruct.2014.10.028
24. Arani AG, Shahraki ME, Haghparast E (2022) Instability analysis of axially moving sandwich plates with magnetorheological elastomer core and GNP-reinforced face sheets. J Braz Soc Mechan Sci Eng 44:150. https://doi.org/10.1007/s40430-022-03446-6
25. Eloy FS, Gomes GF, Ancelotti AC Jr, Cunha SS Jr, Bombard AJF, Junqueira DM (2018) Experimental dynamic analysis of composite sandwich beams with magnetorheological honeycomb core. Eng Struct 176:231–242. https://doi.org/10.1016/j.engstruct.2018.08.101
26. Fadaee M, Talebitooti M (2019) Dynamic stability of the rotating carbon nanotube-reinforced adaptive sandwich beams with magnetorheological elastomer core. J Sandw Struct Mater 23(3):931. https://doi.org/10.1177/1099636219849414

27. Bastola AK, Hossain M (2020) A review on magneto-mechanical characterizations of magnetorheological elastomers. Compos Part B Eng 200:108348. https://doi.org/10.1016/j.compositesb.2020.108348
28. Moreno-Mateos MA, Lopez-Donaire ML, Hossain M, Garcia-Gonzalez D (2022) Effects of soft and hard magnetic particles on the mechanical performance of ultra-soft magnetorheological elastomers. Smart Mater Struct 31(6):65018. https://doi.org/10.1088/1361-665X/ac6bd3
29. Bastola AK, Hossain M (2021) The shape–morphing performance of magnetoactive soft materials. Mater Des 211:110172. https://doi.org/10.1016/j.matdes.2021.110172
30. Lucarini S, Hossain M, Garcia-Gonzalez D (2022) Recent advances in hard-magnetic soft composites: synthesis, characterisation, computational modelling, and applications. Compos Struct 279:114800. https://doi.org/10.1016/j.compstruct.2021.114800
31. Yarali E, Baniasadi M, Zolfagharian A, Chavoshi M, Arefi F, Hossain M, Bastola A, Ansari M, Foyouzat A, Dabbagh A, Ebrahimi M, Mirzaali MJ, Bodaghi M (2022) Magneto-electro-responsive polymers toward manufacturing, characterization, and biomedical soft robotic applications. Appl Mater Today 26:101306. https://doi.org/10.1016/j.apmt.2021.101306
32. Hou S, Li M, Luo J, Kiani Y (2023) Numerical modeling of vibration and damping of higher-order magnetorheological elastomer polar orthotropic composite sectorial annular plates. Thin-Walled Struct 188:110825. https://doi.org/10.1016/j.tws.2023.110825
33. Navazi HM, Bornassi S, Haddadpour H (2017) Vibration analysis of a rotating magnetorheological tapered sandwich beam. Int J Mech Sci 122:308–317. https://doi.org/10.1016/j.ijmecsci.2017.01.016
34. Li H, Wang W, Wang X, Han Q, Liu J, Qin Z, Xiong J, Guan Z (2020) A nonlinear analytical model of composite plate structure with an MRE function layer considering in/ternal magnetic and temperature fields. Comp Sci Technol 200:108445. https://doi.org/10.1016/j.compscitech.2020.108445
35. Kumar M, Kar VR, Chandravanshi ML (2022) Free vibration analysis of sandwich composite plate with honeycomb core. Mater Today Proc 56(2):931–935. https://doi.org/10.1016/j.matpr.2022.02.561
36. Şakar G, Bolat FC (2015) The free vibration analysis of honeycomb sandwich beam using 3D and continuum model. Int J Mechan Mechatr Eng 9(6):828
37. Tourab M, Aguib S (2019) Experimental analysis of the thermal effect of the magneto-mechanical behavior of viscoelastic elastomer. J Adv Res Fluid Mechan Thermal Sci 53(1):25–34
38. Nayak B, Dwivedy SK, Murthy KSRK (2014) Dynamic stability of a rotating sandwich beam with magnetorheological elastomer core. Eur J Mech A/Solids 47:143–155. https://doi.org/10.1016/j.euromechsol.2014.03.004
39. Boczkowska A, Awietjan SF, Pietrzko S, Kurzydłowski KJ (2012) Mechanical properties of magnetorheological elastomers under shear deformation. Compos B Eng 43(2):636–640. https://doi.org/10.1016/j.compositesb.2011.08.026
40. Aguib S, Nour A, Benkoussas B, Tawfiq I, Djedid T, Chikh N (2016) Numerical simulation of the nonlinear static behavior of composite sandwich beams with a magnetorheological elastomer core. Compos Struct 139:111–119. https://doi.org/10.1016/j.compstruct.2015.11.075
41. Scarpa F, Tomlinson G (2000) Theoretical characteristics of the vibration of sandwich plates with in-plane negative poisson's ratio values. J Sound Vib 230:45–67. https://doi.org/10.1006/jsvi.1999.2600
42. Xiao Y, Wen XD, Liang D (2021) Failure modes and energy absorption mechanism of CFRP thin-walled square beams filled with aluminum honeycomb under dynamic impact. Comp Struct 271:114159. https://doi.org/10.1016/j.compstruct.2021.114159
43. Li Z, Wang Z, Wang X, Zhou W (2020) Bending behavior of sandwich beam with tailored hierarchical honeycomb cores. Thin-Walled Struct 157:107001. https://doi.org/10.1016/j.tws.2020.107001
44. Fu Y, Sadeghian P (2020) Flexural and shear characteristics of bio-based sandwich beams made of hollow and foam-filled paper honeycomb cores and flax fiber composite skins. Thin-Walled Struct 153:106834. https://doi.org/10.1016/j.tws.2020.106834
45. Kolařík J, Pegoretti A (2006) Non-linear tensile creep of polypropylene: time-strain superposition and creep prediction. Polymer 47(11):346–356. https://doi.org/10.1016/j.polymer.2005.11.013
46. Madigosky WM, Lee GF (1983) Improved resonance technique for materials characterization. J Acoust Soc Am 73(14):1374–1377. https://doi.org/10.1121/1.389242
47. Wang N, Deng Q (2021) Efect of axial deformation on elastic properties of irregular honeycomb structure. Chin J Mechan Eng 34(51):574. https://doi.org/10.1186/s10033-021-00574-3